Landslides (2020) 17:419–431
DOI 10.1007/s10346-019-01317-1
Received: 27 March 2019
Accepted: 5 November 2019
Published online: 26 November 2019

Jiajia Wang · Lili Xiao · Jun Zhang · Yanbo Zhu

Deformation characteristics and failure mechanisms of a rainfall-induced complex landslide in Wanzhou County, Three Gorges Reservoir, China

Abstract A rainfall-induced complex landslide occurred on April 4, 2013, in Wanzhou County, Three Gorges Reservoir, China. Approximately 1.5 × 10^6 m^3 of earth and rock mass slid over a distance of ~ 30 m, destroying residential buildings and rural roads. We perform a comprehensive assessment of the cause of this landslide using field surveys, borehole drillings, and interpretations of aerial photographs. This landslide exhibited a complex failure mode in which the upper part of the earth slope first deformed and slid along geotechnical interfaces. This then triggered the slide of the lower part of the flysch bedding rock. In this study, the landslide mass was divided into nine separate blocks considering their internal geological features and movements. The study also shows that antecedent rainfall, in association with the geological and morphological features of the steep slope, the presence of weak interlayers, and human interventions such as slope excavations, jointly caused this disaster. This well-observed event study facilitates comprehensive recognition of the deformation characteristics and failure mechanisms of rainfall-induced complex landslides and also provides an insight into landslide hazard mitigation.

Keywords Complex landslides · Antecedent rainfall · Deformation characteristics · Failure mechanism · Hazard mitigation

Introduction

Rainfall-induced landslides, recognized as one of the most frequent natural hazards, often cluster regionally with substantial negative consequences (Baum and Godt 2010; Cruden and Varnes 1996). Adverse geological conditions and human activities may exacerbate hazardous situations (Crosta and Frattini 2008). Brief and intense rainfall often generates shallow soil landslides, those with slope deformation concentrated in the surface layers (Cannon 1985; Dai and Lee 2001; Michiue 1985). Rainfall infiltration increases pore pressure, decreases the effective stress in the soil, and reduces shear strength, eventually resulting in slope failure (Reid 1994; Terzaghi 1950; Wang and Sassa 2003). In contrast, deep-seated landslides are mostly triggered by a prolonged, low intensity rainfall that leads to large bedding rockslides and colluvial landslides where the sliding surface is located at deeper weak interlayers (Hong et al. 2005). In these situations, decreasing slope matrix suction and rainfall softening of the weak interlayers are regarded as the main reasons for slope deformation and failure (Bonnard and Noverraz 2001; Capparelli and Tiranti 2010).

Rainfall-induced complex and large landslides represent a persistent threat to settlements and infrastructures in mountainous areas worldwide (Conte et al. 2017; Duc 2013; Martha et al. 2015; Xu et al. 2012). Varnes (1958, 1978) proposed a comprehensive system of landslide classification that has widely been agreed upon by international researchers and practitioners. Complex landslides are defined as those with multiple types of material components (rock, soil, or debris), motion styles, and mechanisms (fall, topple, sliding, spreading and flow, or retrogressive and load-caused types). Complex landslides need to be investigated both from the surface and at depth to understand the geomorphological and geological properties that lead to the corresponding deformation mechanisms. These mechanisms are the key to quantifying the future development and evolution of landslides (Sabatakakis et al. 2005; Brambilla et al. 2017; Lin et al. 2018).

Wanzhou County is one of the most geologically disaster-prone areas in the Three Gorges Reservoir region, China. Landslides that occur here are frequent, high density, and widely distributed (Wang 2015). The deformation mechanisms of rainfall-induced landslides in this area are complex, due to various geological and climatic conditions and human activities (Ma et al. 2018; Santo et al. 2018). On April 4, 2013, the Sunjia landslide, a complex landslide with a volume of approximately 1.5 × 10^6 m^3, occurred on the western border of Wanzhou County. Triggered by heavy rainfall, the upper-earth slope first deformed along a geotechnical interface, which then induced sliding of lower flysch bedding. The landslide traveled nearly 30 m horizontally, destroying all of the residential buildings and rural roads in its path. Post-slide deposits remain unstable, threatening the lives and properties of residents downslope. Comprehensive studies of landslide deformation processes and failure mechanisms are urgently required for hazard mitigation and control of the Sunjia landslide.

In this study, we investigate the physiography and geological settings, deformation characteristics, and failure mechanisms of the Sunjia landslide based on field surveys, drilled boreholes, and aerial photography. The comprehensive study provides insights into rainfall-induced complex landslides, as well as guidance for the prevention and reduction of landslide hazard and risk.

Background

At about 13:15 on April 4, 2013, a landslide with a volume of approximately 1.5 × 10^6 m^3 occurred at the northwest wing of the Tiefeng mountain anticline, located within the administrative jurisdiction of Sunjia town, 42 km west of the capital of Wanzhou County, Three Gorges Reservoir, China (Fig. 1). The landslide traveled nearly 30 m horizontally in a N-S direction and destroyed several rural roads and residential buildings (Figs. 2 and 3). Thanks to an early warning of the disaster, no one was killed nor injured. However, the extremely unstable slope of the post-slide deposits still threatens the lives and properties of the local residents and a 450-m section of the Yuwan national expressway.

The first field survey of the site was carried out one day after the slope failure (April 5, 2013). Two supplementary field investigations were conducted in the following two months. The aerial images and fourteen holes drilled by the Nanjiang Hydrogeological Engineering Geological Team contribute to our motion study of the landslide.

Geomorphology of the pre-landslide slope

The landslide is located in low to middle elevation mountains with a slope dipping north at an angle of 20 to 35°. The upper slope is comparatively gentler than the lower part (Figs. 2 and 3). The

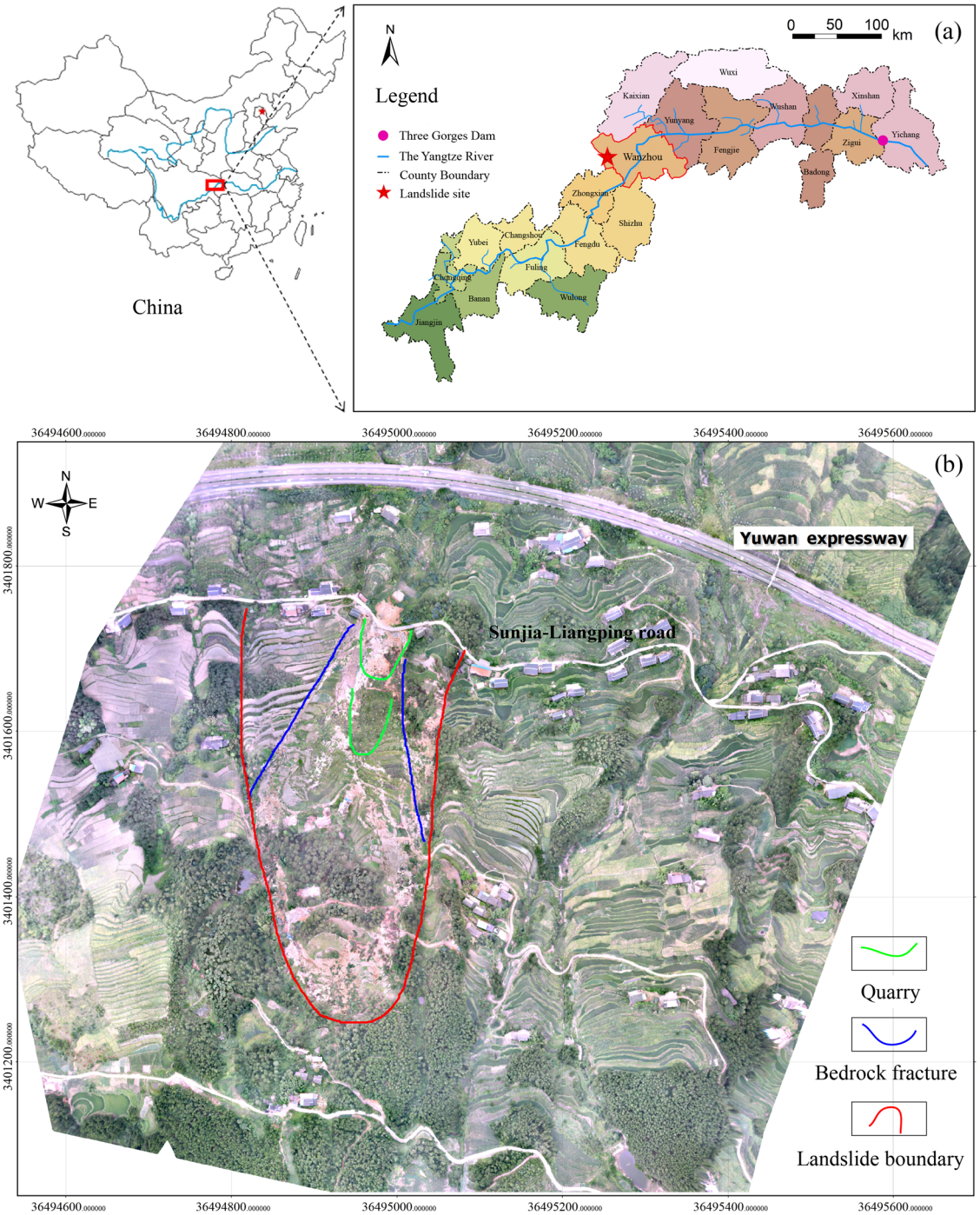

Fig. 1 Location of the study site. **a** The Three Gorges Reservoir area. **b** A post-event aerial image of the landslide site collected from the Nanjiang Hydrogeological Engineering Geological Team

landslide headscarp emerged near a country road at an elevation of 960 to 962 m a.s.l. (above sea level), and the landslide toe is at an elevation of 787 to 800 m a.s.l. at the inner side of the Sunjia-Liangping road (Fig. 2). Two N-S orientated gullies developed on both sides of the landslide with a depth of 5 to 10 m, a width of 4 to 9 m, and a length of about 1500 m, exposing a clear sequence of the stratum lithology (Figs. 1b and 2). There is also an abandoned quarry which served the construction of the Yuwan expressway and, below this, a slope excavation that resulted from building the Sunjia-Liangping road several years previously. These form a two-stage cutting slope at the landslide toe, each having a slope height of 10 to 15 m, a slope angle of 50 to 70°, and volumes of 1500 and 2000 m^3 (Figs. 2 and 10). Both of these features provide favorable geomorphic conditions for the slope failure.

Hydrogeology and climatic conditions

The groundwater of the Sunjia slope is mainly replenished by precipitations through surface infiltration and fluctuates

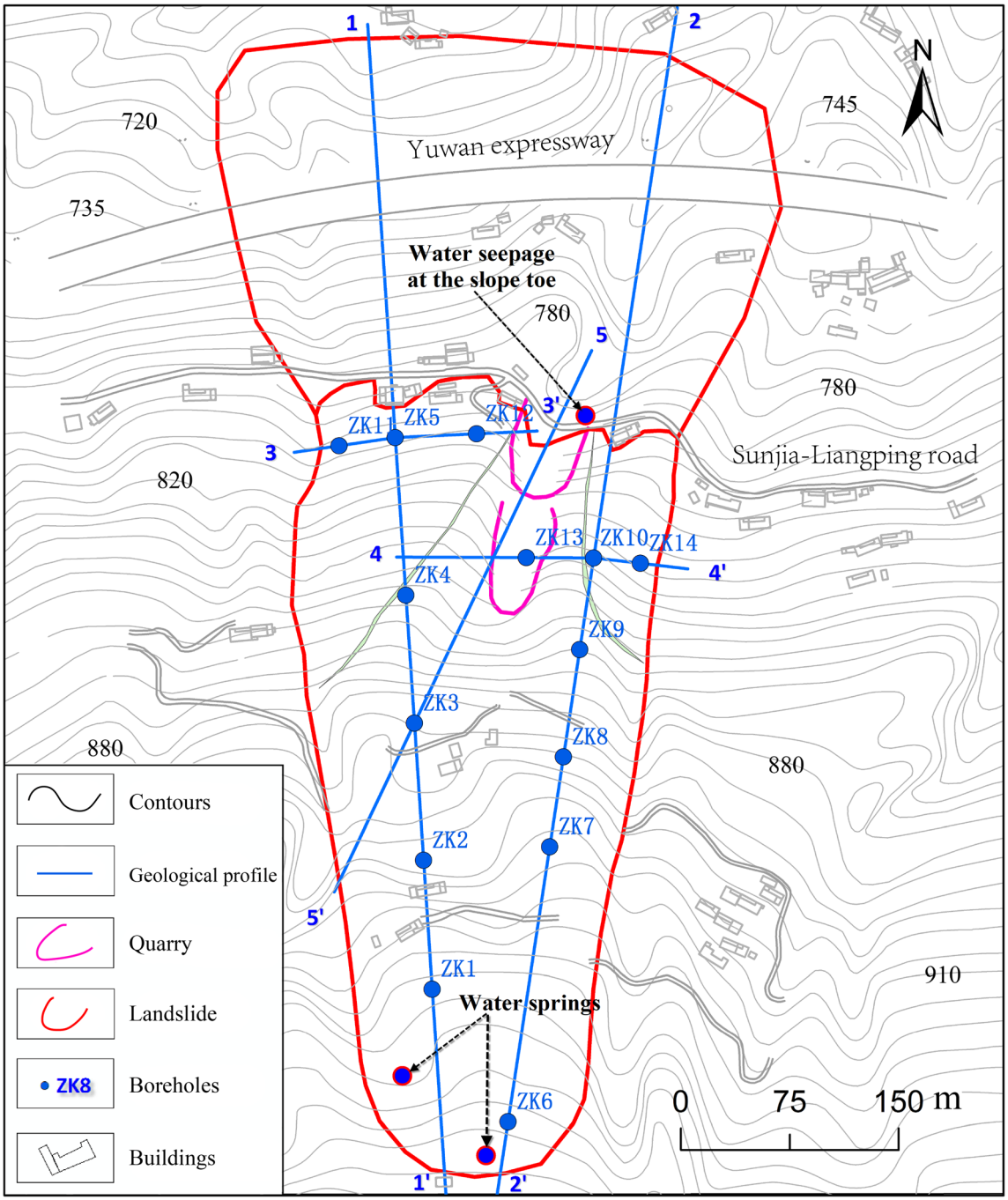

Fig. 2 Geological ichnography of the Sunjia landslide. The blue numbers are the serial numbers of the boreholes. The black numbers mark the elevations of the contours (5 m)

seasonally with rainfall. In order from the top, the soil profile comprises the following: fragmented stone soil, weathered sandstone, and finally the flysch stratum of sandstone and shale. The upper layer is relatively permeable and allows water to pass through, whereas the underlying shale stratum could be considered impermeable. Therefore, the groundwater level of the landslide increases during the wet season, with most of the water runoff and discharge tracing the steep slope in a N-S direction towards the lower toe. Some of the groundwater is discharged as spring water in a low depression at the back margin of the landslide and other seeps at the foot of the steep slope at the front edge of the landslide (Fig. 4). Figure 2 shows the locations of the water springs and water seepage.

The study area situates in a subtropical zone that has a continental climate influenced by monsoons, with the weather warm and humid in summer. Rainfall is abundant and synchronous with heat; 60 to 70% of the annual rainfall occur between May and September. The average and maximum annual precipitation measure 1191.3 mm and 1635.2 mm over the past 50 years. The

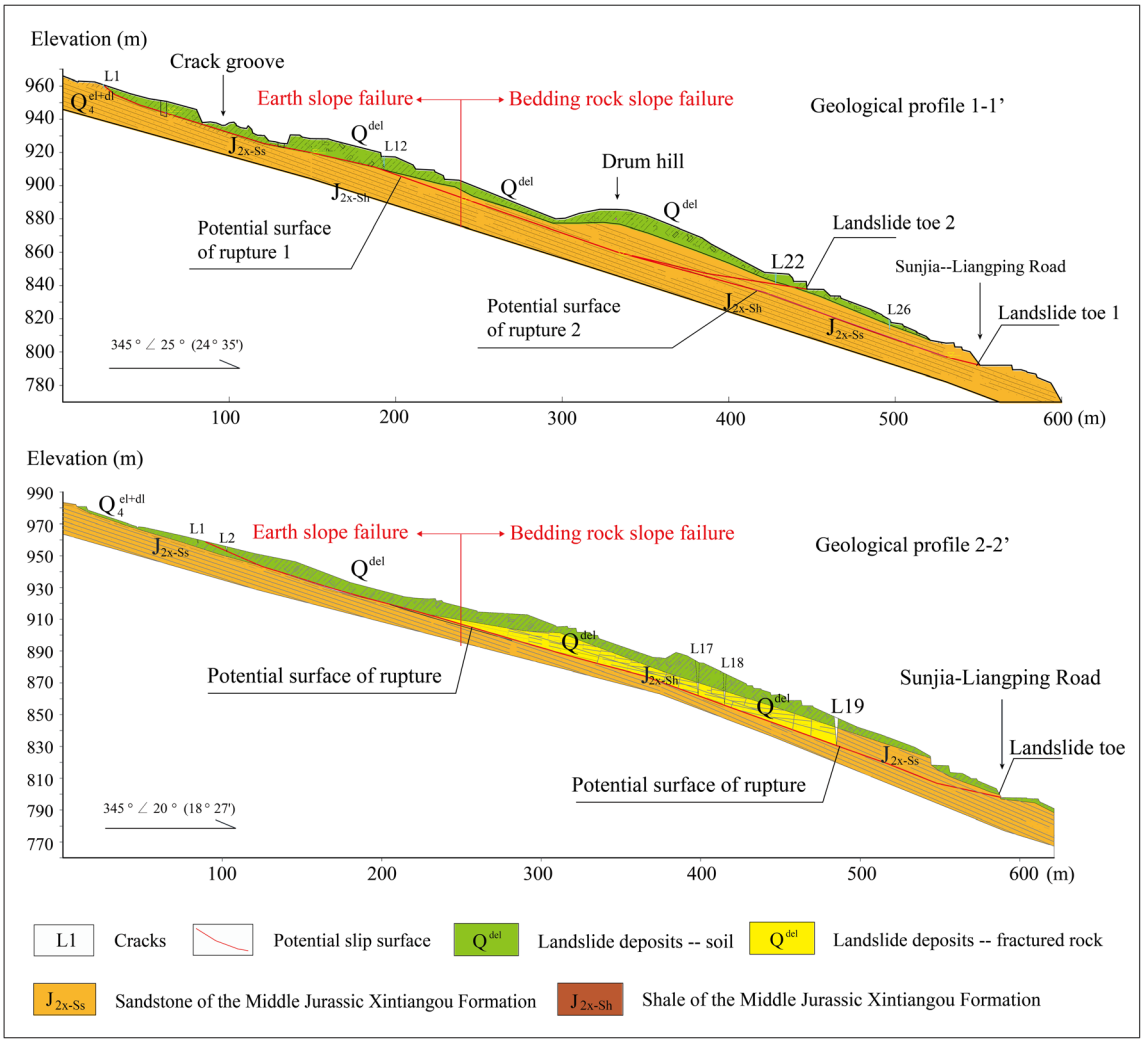

Fig. 3 Geological profile 1-1′ and 2-2′ of the Sunjia landslide (see Fig. 2 for the locations of the profiles)

maximum daily rainfall in this region was 243.31 mm (July 16, 1982), and the maximum continuous precipitation lasted for 16 days. The rainfall frequency increased from March 10 to 26, 2013, and the maximum daily rainfall reached over 30 mm. The antecedent rainfall at that time could be the main factor that induced the failure of the Sunjia slope (Fig. 5).

Fig. 4 Photographs taken by the authors showing. **a** Water spring at the back margin of the landslide. **b** Water seepage at the slope toe (see Fig. 2 for the locations of the photo taken)

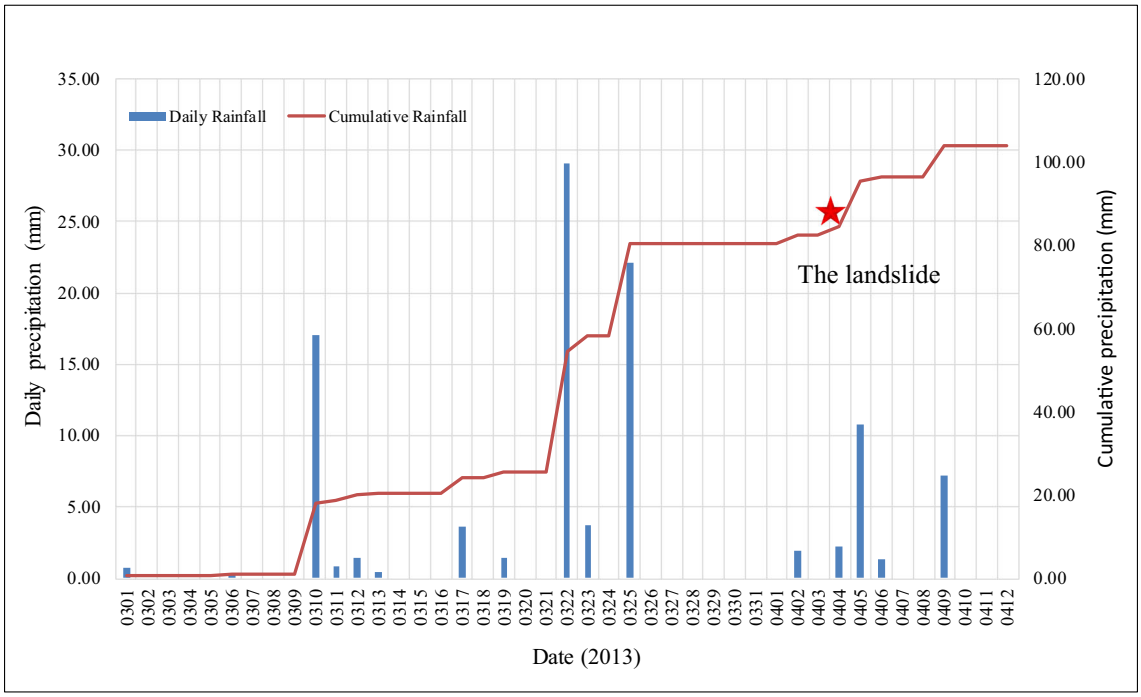

Fig. 5 Distribution of daily average precipitation from March 1 to April 12. The red star marks when the Sunjia landslide occurred (data collected from the Wanzhou Geological Environment Monitoring Station)

Stratigraphic setting

The landslide initiated at the north-west wing of the Tiefeng mountain anticline. The bedrock here dips NW at an angle of 20 to 25°. According to the field surveys, borehole data, and previous geological reports (Geological survey, 2013, unpublished report), the lithology of the landslide primarily consists of the overlying Quaternary-Holocene accumulation of eluvium silty clay (Q_4^{el+dl}), landslide accumulation (Q^{del}), and the underlying bedrock of the Xintiangou Formation of the Lower Jurassic (J_{2x}).

The eluvium silty clay (Q_4^{el+dl}) has a thickness of 0.5 to 5 m and contains a small amount of gravel taking up 10 to 25% of the layer. The landslide accumulation (Q^{del}) is primarily the debris soil and fractured rock mass of the post-landslide deposits. The fractured rock is fresh with block diameters ranging from about 3 to 75 cm.

The Xintiangou Formation is mainly composed of gray sandstone (1.6 to 25.5 m thick) and shale (0.3 to 4.6 m thick) with a strongly weathered layer of thickness 0.5 to 1.95 m. The gray sandstone has a medium-coarse grain structure and consists of quartz, feldspar, calcium, and argillaceous cementation. The strong weathered layer of shale with a thin and muddy structure presents a soft layer with weak resistance to weathering.

Distribution of weak interlayers

Two groups of rock fractures developed in the sandstone within the landslide (Figs. 1b and 2). Both fractures L22 and L19 are a swarm of closely spaced, parallel or sub-parallel, overlapping cracks with lengths ranging from 1 to 20 m and spacing between 1 and 5 m. Fracture L22 dips east at an angle of 70 to 85° and a width of 1 to 100 mm (with a maximum of 300 mm). Fracture L19 dips south at an angle of 75 to 87° and a width of 1 to 100 mm (and a maximum of 400 mm). Both fractures are considered to be weak structures with rough surfaces that filled with muddy packing with poor bonding strength.

The layer between the sandstone and shale is a muddy cementation with flat and smooth crack surfaces and poor bonding strength. The unfavorable physical and mechanical properties of this weak structural surface in terms of shear resistance are likely to stimulate potential slope failure in the event of changes in the external conditions, such as excavations and rainfall infiltration. We conclude that the slope deformation is mainly determined by these discontinuous weak interlayers.

Deformation process and characteristics

At 18:00 on April 3, 2013, the landslide began, with slight cracking starting to appear in the walls and around some of the houses in the middle and rear part of the landslide. During the morning of April 4, landslide deformation intensified. A large number of ground fissures were found at the top of the slope, with lengths extending from 1 to 20 m and widths from 0.2 to 10 cm. The residential buildings were also experiencing serious cracking, accompanied by noise, with the situation obviously deteriorating. Extensive sliding began at 13:15 on April 4, and the landslide almost stopped by the morning of April 5, with a maximum runout distance of 29.5 m.

Deformation characteristics based on field survey

The landform topography had changed significantly after the slope failure, presenting a large number of cracks, a surface bulge (drum hill), ground fissures, and the collapse of rural roads and residential buildings (Fig. 6). The slip of the upper-earth slope formed two tensile cracks, one of which is along the landslide back margin (Fig. 6, region A) with a width of ~ 67 m, longitudinal length of ~ 160 m, and a depth of ~ 10 m (Fig. 7a). Another tensile crack at the right boundary of the landslide (Fig. 6, region B) is about 5 to 10 m

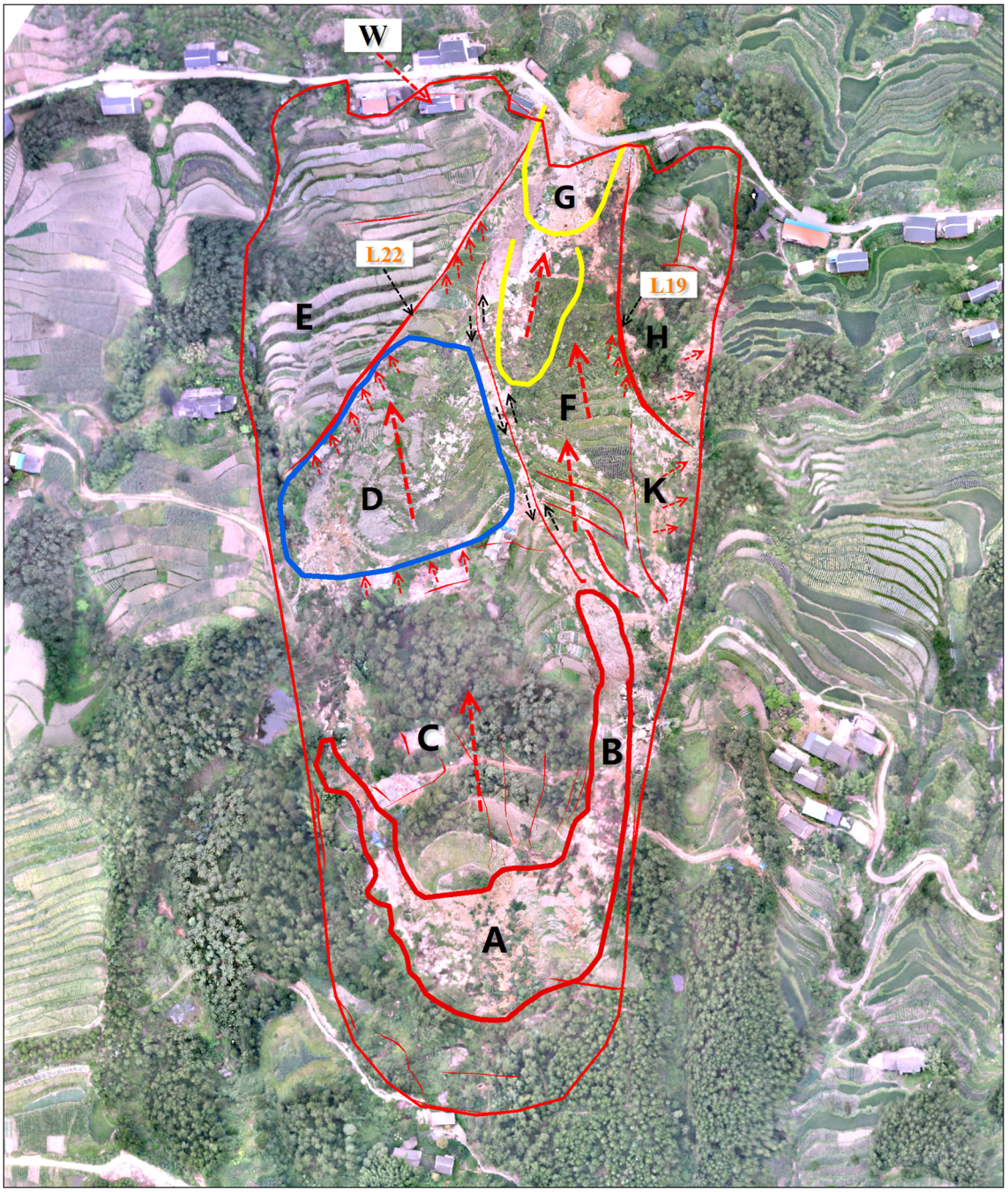

Fig. 6 Interpretation of the landslide deformation extent based on aerial images. Note the lettering indicates different regions where photographs presented in this paper have been taken (see Figs. 7 and 8)

in width, ~ 220 m in longitudinal length, and ~ 5 m in depth (Fig. 7b). Influenced by the two tensile cracks, a rural road along the rear part of the landslide was dislocated downward by a vertical height of approximately 6 m and a distance of about 29.5 m (Fig. 7c). In addition to the large cracking grooves, other ground cracks were generated in the middle part of the landslide, reaching a maximum length of ~ 50 m, a width of ~ 3 m, and a depth of ~ 5 m (Figs. 6, red lines and 7d).

The ground in the middle of the landslide was blocked by the bedrock at the boundary of fracture L22 (Fig. 6, L22). The landslide then warps upward, forming a drum hill about 110 m wide, 55 m long, and 4 to 5 m high, that is mostly comprised of argillaceous siltstone and has undergone mechanical breaking (Figs. 8a and 10, geological profile 5-5'). The process of forming the drumhead and depression in region D, as well as the impact and accumulation process in regions F and G, had an adverse impact on the bedrock at the boundary of the fracture L22 in region E (Fig. 6). The intense impact resulted in the local weak deformation of the thin soil layer overlying the bedrock in region E (Fig. 6). According to eyewitness description, the relatively weak foundation of the front structure

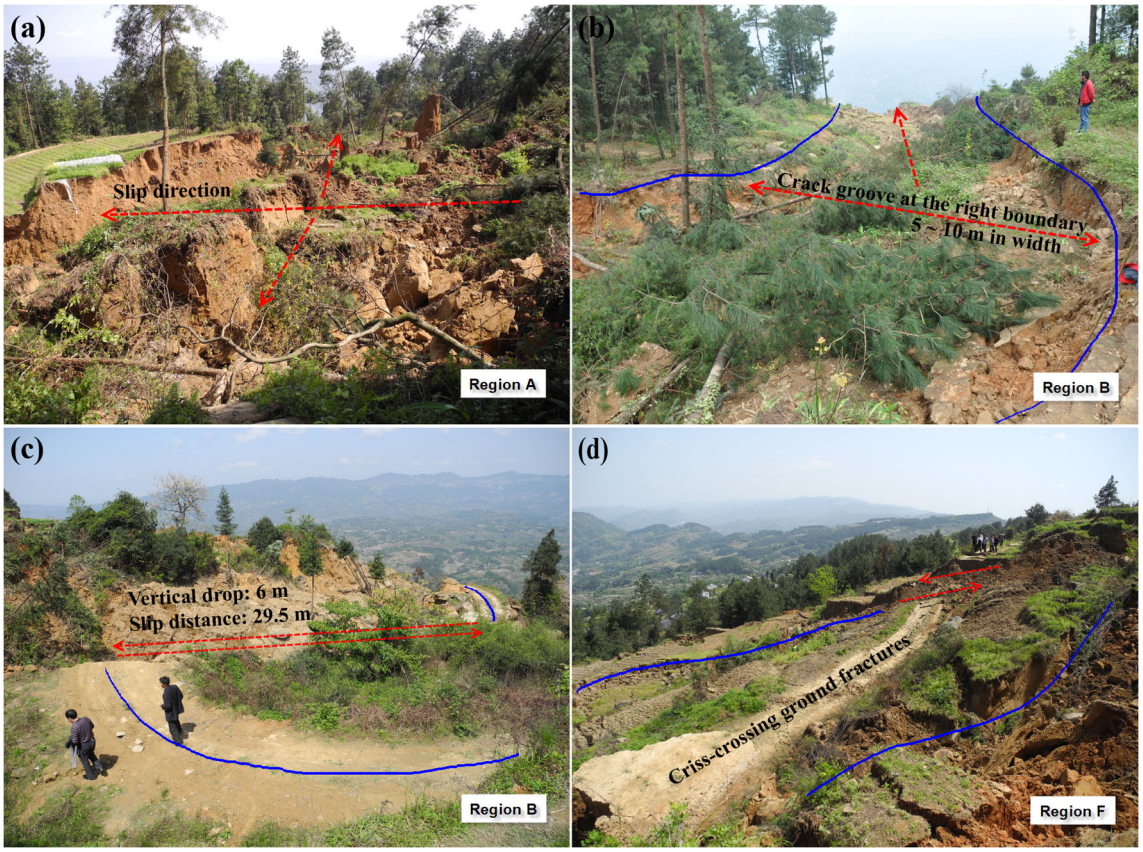

Fig. 7 Photographs taken by the authors showing the landslide's deformation characteristics. **a** The tensile crack at the back margin of the landslide in region A. **b** The tensile crack at the right-hand side boundary of the landslide in region B. **c** The dislocation downwards of the rural road in region B. **d** Criss-crossing ground fractures that developed in region F. The locations of the photos taken are marked in Fig. 9

of the residential building W near the Sunjia-Liangping road in region E (Fig. 6) was destroyed in the course of the landslide, while the main body of the house remained intact (Fig. 8b). In consideration of this and the deformation characteristics of the landslide, we hold the opinion that the shaking force caused by this impact on the residential building lead to the collapse of the house foundation.

Pushed by the upper-earth slope failure in the back margin, the lower part rock mass (Fig. 6, region F) slid forward along the weak interlayer between the sandstone and the shale located by the borehole data. Controlled and blocked by the structural fracture L19 (Fig. 6), the rock mass with overlaying soil on the middle-right side of region F and K slid towards the quarry and deposited most of its material there (Figs. 6, region G and 8c). The differential movements of the slide in regions D and F produced a long shearing crack between the two regions (Fig. 6). Some of the overlaying soil disintegrated and crashed into the right-side gully (Figs. 6, region K and 8d). With respect to topographic conditions, a small part of the slide overshot the boundary of fracture L19 and accumulated in the weak deformation region H (Fig. 6). The extruding mass movement generated bulging cracks at the landslide toe and squeezed a thin layer of shale at the front, forming an undulating shape (Fig. 8e). The residential buildings on the landslide suffered the most serious damage and some collapsed (Fig. 8f). After the event, the main slope still continuously creeps and the steeper slope shows greater deformation, indicating the potential instability of the post-slide slope.

Deformation division of the Sunjia landslide

Restricted by the topographic conditions, structural planes, and thickness changes of the weathering layer, the landslide displayed significant disintegration during the sliding. Based on the deformation characteristics described previously and the geological profiles derived from borehole data, the post-landslide area was divided into nine deformation zones (Fig. 9).

The zone of the tensile grooves at the back margin of the landslide (zone I): This area was strongly affected by the deformation of the tensile grooves in zone II and developed a number of cracks due to large displacement earth-slope failure (Fig. 7a). The elevation of this zone at the back margin of the landslide is about 950 m a.s.l. Zone I narrows gradually from the main axis of the landslide towards both sides. The width of the central area is about 30 m. The main cracks strike perpendicular to the main slide direction and parallel to the back scarp of the landslide. Based on the characteristics of the crack width, extension direction, and cutting relation, we believe that this area is still in an unstable state and is likely to develop local collapse.

The fractured zone of the tensile groove at the back margin of the landslide (zone II): The elevation of this zone is between 940 and 950 m a.s.l. During landslide initiation, a number of

Fig. 8 Photographs taken by the authors showing the landslide deformation characteristics. **a** The drum mound formed by the landslide's extrusion in region D. **b** The house foundation that collapsed due to the bedrock collision in region W. **c** Landslide deposits in the quarry. **d** Slope deformation in region K. **e** Undulating deformation of the shale rock at the left-side of the landslide toe in region G. **f** Dilapidated houses in the upper part of the slide in region C. The locations of the photos taken are marked in Fig. 9

preponderant arc tensile cracks appeared and finally connected, tearing the vegetation covering of the slope here. The tensile cracks gradually widened and collapsed, forming a U-shape tensile groove along the rear edge of the slide (Figs. 6, regions A and B 7a, b). The width of the tensile groove reached up to 67 m near the main axis line and decreased from the middle towards both edges (Fig. 9). This zone of tensile groove provides evidence of the overall sliding of the upper-earth slope with a maximum distance of ~ 30 m.

Complete slip zone of the upper-earth slope (zone III): The elevation of this zone is between 882 and 940 m (Fig. 6, region C). The drilling survey shows that the earth landslide is about 300 m long and 15 m in depth with an average width of about 200 m (Fig. 3). Pine forests and other vegetation are well developed in this area, and most of the residential buildings are distributed on this platform. The left-front side of this zone was blocked during the landslide movement by the central-left thrust nappe, and as a result, very few cracks developed here. By contrast, broken trees and surface cracks are widely distributed on the right-front side of this zone adjacent to the right-wing gully (Fig. 6, region K). Variations in slip distance at different sections produced cracks with variable lengths during the movement (Fig. 7d).

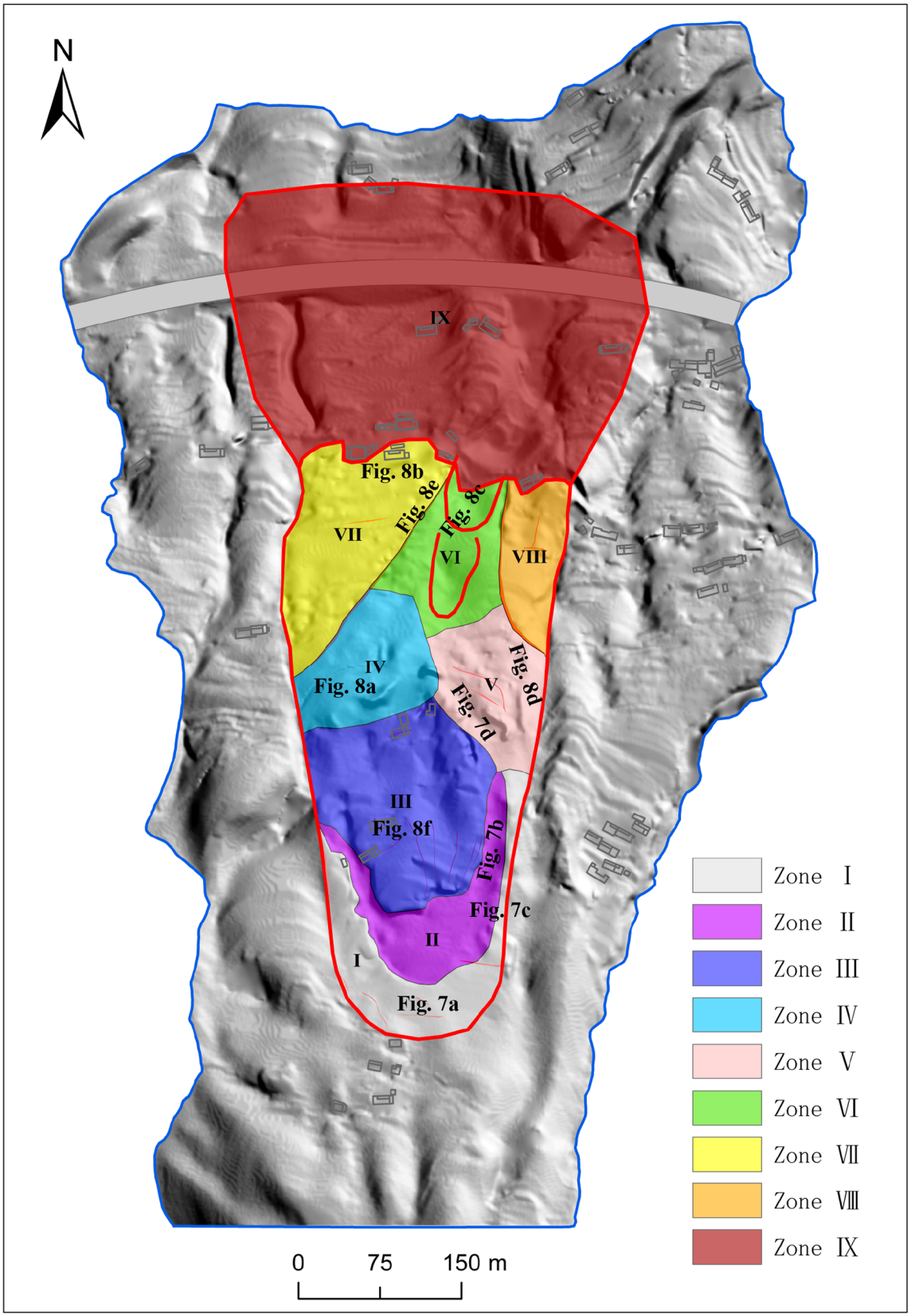

Fig. 9 The subdivision of the deformation of the Sunjia landslide. The annotations mark the locations of the photos presented in Figs. 7 and 8

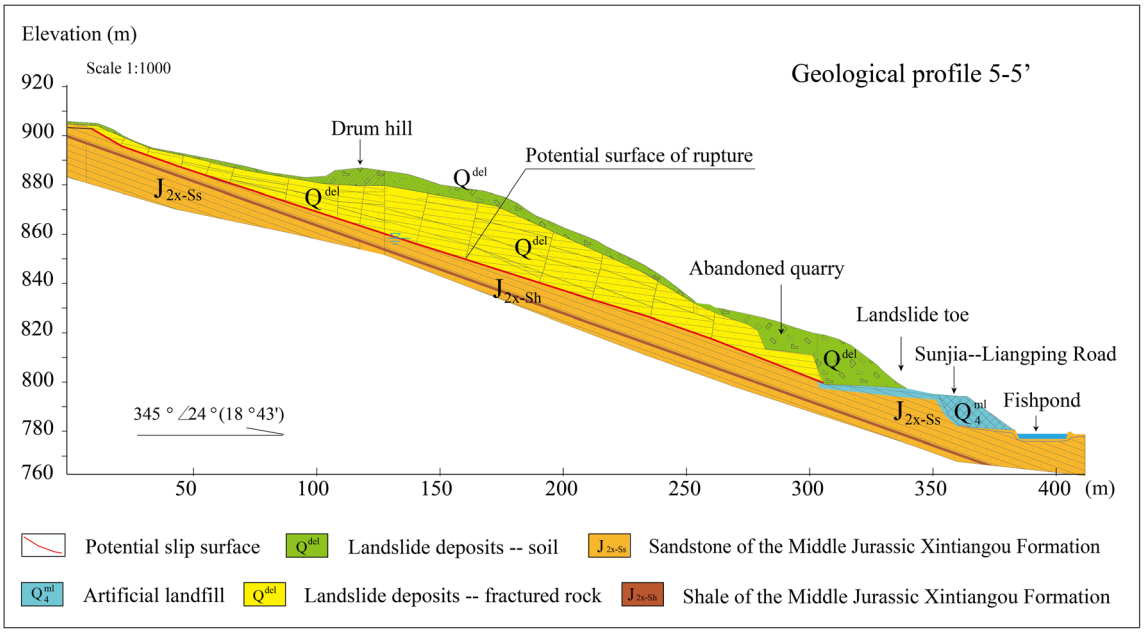

Fig. 10 Geological profile 5-5' (see Fig. 2 for the location of the profile)

The thrust nappe area in the central part of landslide (zones IV and V): The elevation of the thrust nappe area is between 857 and 885 m. Based on the field surveys, we divided this area into right and left parts (Fig. 9, zones IV and V), which are bounded by a shearing crack striking southeast to the northwest between regions D and F (Fig. 6). Blocked by stable bedrock at the outside of fracture L22, the left part (zone IV) experienced intense collisions and extrusions, leading to an obvious topographic uplift of about 6 m compared to the original landform (Fig. 8a). Blocked by stable bedrock at the outside of fracture L19 and influenced by the lower free surfaces of the quarry and the right-hand gully (Fig. 6, H, G and K), the right part slide (zone V) moved downwards along the confined terrain and deposited in the quarry (Fig. 8c).

Frontal accumulation zone (zone VI): The accumulation area is mainly located in the quarry at the landslide toe (Fig. 10, geological profile 5-5'). A large amount of fractured sandstone and shale mixed with argillaceous siltstone and weathered Quaternary soil were deposited in this area (Fig. 8c). The elevation of the accumulation area is relatively lower than the stable area on both sides, with a stacking thickness of about 20 m (Fig. 11, geological profile 4-4').

Weak deformation zone (zones VII and VIII): The bedrock in this region is relatively intact (Fig. 11, geological profile 3-3'). Impacted by the thrust nappe area (zones IV and V), the overlaying soil in this zone suffered deformation with sporadic fractures. Due to the steep terrain and intense strike at the thrust nappe zones, some of the Quaternary soil on the surface directly crossed the boundary of fractures L19 and L22 and accumulated on the weak deformation zones (Fig. 6).

Landslide potential threat area (zone IX): We find no evidence of mass deformation and destruction in this area after the slope failure in 2013. According to the borehole data and post-event monitoring, the post-slide deposits with a large volume of broken Quaternary debris show an unstable state. An extreme rainfall event would potentially induce the landslide to slip again, threatening the communities downslope (Fig. 10).

Triggering factors and failure mechanism

Factors that induced the Sunjia landslide

Based on field investigation, a drilling survey, and the analysis of landslide deformation characteristics, we discuss below the main factors that caused the Sunjia landslide.

Geomorphic condition: The Sunjia landslide initiated on a steep slope with a slope dipping north at an angle of 20 to 30°. The lower rock slope with a structure of flysch bedding planes was comparatively steeper than the upper-earth slope comprised of a thick layer of soil mixed with gravel. In addition, two large gullies on each side separated the steep slope from the adjacent geomorphic unit, which provided free surfaces for progressive deformation of the slope. With these geomorphic characteristics, the whole slope exhibited limited equilibrium under normal conditions.

Geological structure of the slope: The upper-earth slope is comprised of a loose and porous soil layer overlying the impermeable shale bedrock, which makes it favorable for surface water infiltration and groundwater retention. Moreover, the bedding structure of the lower rock slope with a thin layer of shale beneath the sandstone has a direct influence on the instability of the rock slope, due to an easy formation of a shear slipping surface along the weak interlayers. In addition, the flysch bedding structure of the overlying hard rock (sandstone) and underlying soft rock (shale), of the landslide-prone stratum, was also extremely sensitive to water infiltration and ultimately could be responsible for the formation of the rockslide.

Previous slope excavations: The main engineering activities were excavations at the slope toe in two different periods. The upper excavation was for the construction of the Yuwan expressway several years prior that left an abandoned quarry. The lower one was a later excavation associated with the building of the Sunjia-Liangping road. The two open-pit excavations with volumes of 1500 m^3 and 2000 m^3 formed a two-stage cutting slope at the landslide toe (Fig. 10). Those excavations deteriorated the

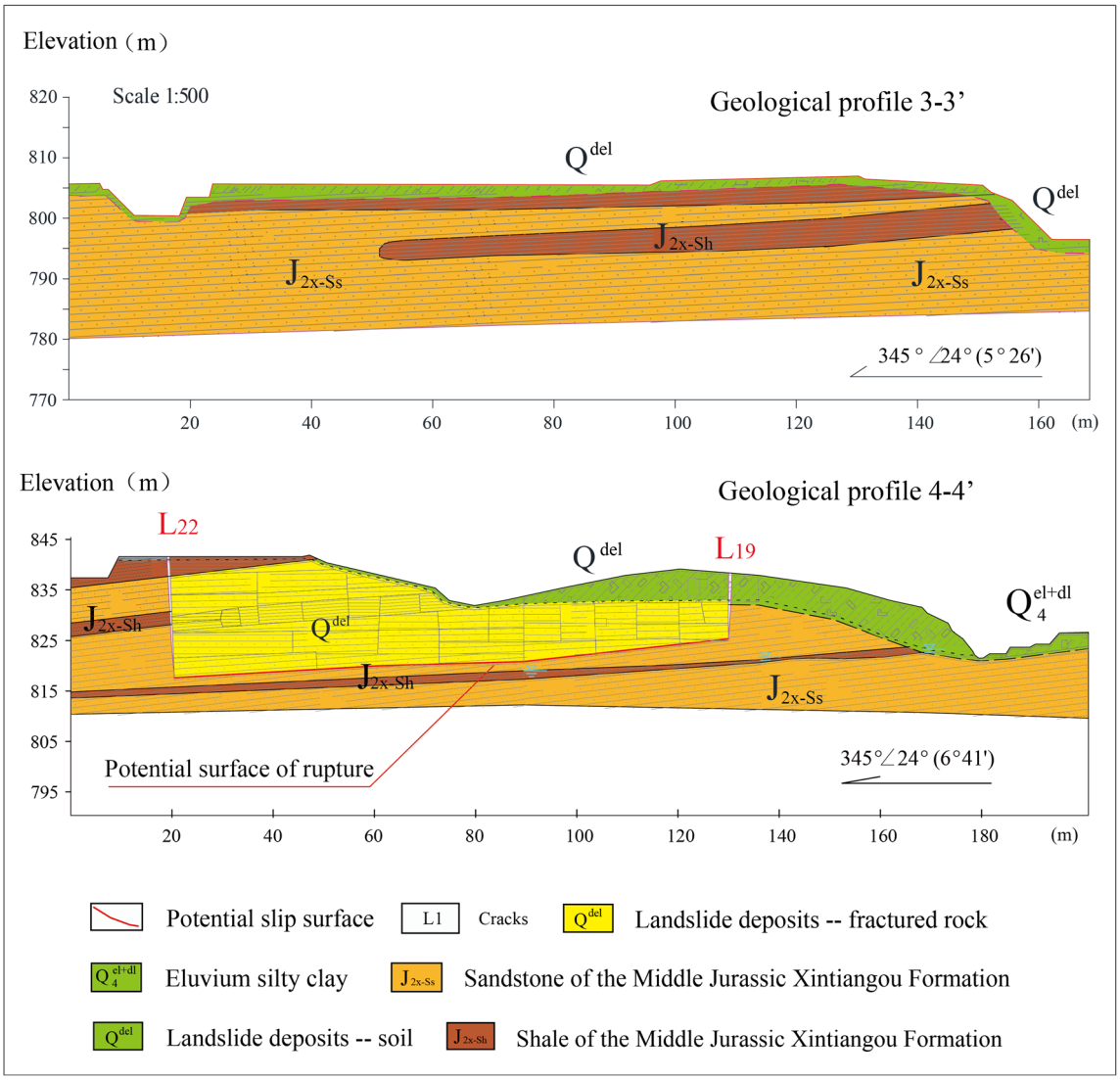

Fig. 11 Geological profiles 3-3′ and 4-4′ (see Fig. 2 for the profiles' locations)

rock mass quality, decreased the retaining force in front of the slope, and drove the lower bedding rock slope from equilibrium towards a disequilibrium/unstable state, which finally contributed to the slope failure.

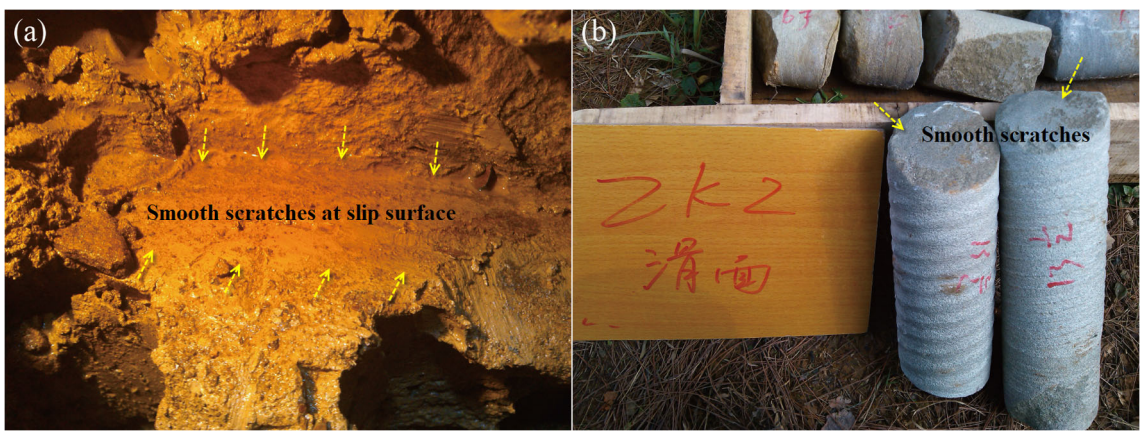

Fig. 12 Slip surfaces exposed by borehole drilling. **a** Slip surface of the earth slope. **b** Slip surface of the bedding rock slope

Antecedent rainfall: It is common knowledge that brief and intense rainfall often generates shallow soil landslides versus deep-seated landslide movements that are mostly triggered by prolonged rainfall of a low intensity. From March 10 to 26, 2013, the rainfall frequency increased and the maximum daily rainfall reached over 30 mm. The frequent and continuous heavy rainfall could have led to the sudden increase of groundwater level and pore pressure. The infiltrated water in both the upper-earth slope and the lower-rock slope would markedly soften the material in weak interlayers and contribute to the degradation of its mechanical strength, which eventually influenced the slope stability.

Mechanism analysis

In general, the combination of internal and external factors contributes to the initiation of large-scale soil landslides or rockslides (Regmi et al. 2017). External triggering factors, such as rainfall and slope excavations, usually play a key role in the redistribution of internal stresses that closely relate to the development of the sliding zone and the eventual failure of the slope (Xu et al. 2015). However, even when the triggering factors are essentially the same, different geological settings of the slope lead to diversities of the macroscopic deformation processes and final failure (Zhang et al. 2018). The failure mechanisms of this rainfall-induced complex landslide were sensitive to geomorphic conditions, geological structures, previous slope excavations, and antecedent rainfall. Rainfall was the main triggering factor that increased the pore water pressure and reduced the mechanical strength of the slide mass. It had an adverse impact in driving both the upper-earth slope and the lower bedding rock slope to a disequilibrium/unstable state, resulting in different failure mechanisms and movements constrained by the internal geological settings.

Interviews with eyewitnesses revealed that the upper-earth slope first deformed and slid downwards with a maximum distance of ~ 30 m (Fig. 9, zone III). The permeable porous soil, comprised of silty clay and broken gravel overlying the impermeable bedrock, made surface water infiltration and groundwater retention of prolonged rainfall possible (Fig. 5). The infiltration of about 100 mm of the antecedent rainfall destabilized the soil mass and resulted in the progressive degradation and reduction of its mechanical strength (Goodman and Kieffer 2000). Meanwhile, the water content and pore water pressure increased suddenly, the effective friction angle on the geotechnical interface decreased notably, and the rate of slope deformation accelerated, facilitating the penetration of the sliding surface. The fact that this eventually caused the upper-earth slope failure (Hungr et al. 2014) can be confirmed by the appearance of a flat and smooth slip surface revealed by the drilling survey (Fig. 12a). In addition, the separation of the steep slope from the adjacent geomorphic unit by two gullies also provided good geomorphic conditions for the upper-earth slope failure.

As for the lower bedding rockslide, the flysch bedding planes comprising the overlying hard rock and underlying soft rock provided a slope structure with a tendency for sliding (Figs. 3 and 10). More precisely, a shear sliding surface can easily form along the bedding planes that could be ultimately responsible for the formation of the rockslide (Luo et al. 2012, 2017). Also, rainwater infiltration led to a reduction of the shear strength of the impermeable interlayer of the shale with a muddy structure due to long-term immersion. In addition, the free surface at the toe of the rock slope formed by the previous open-pit excavations had an adverse impact in decreasing the retaining force and driving the slope towards a disequilibrium/unstable state. Pushed by the upper-earth slide, the lower bedding rock slope formed a penetrating shear slip plane at the weak interlayer surface of shale, and quickly transformed into a rock slide (Figs. 10; 11, geological profiles 4-4'; and 12b). However, the two well-connected fractures, L19 and L22 (Fig. 6), that developed on each side of the quarry blocked the main rockslide body and resulted in fragmentation of the bedding rock and limited slipping distance (< 10 m) downslope (Fig. 10, geological profiles 5-5').

Overall, it can be concluded that the Sunjia landslide presented a complex and progressive failure, indicating that the upper-earth slope first deformed along the geotechnical interface and then drove the lower part flysch bedding rock slope to slide along a weak interlayer. The failure mechanisms were determined by both internal (geomorphic condition and slope structure) and external (open-pit excavations and heavy rainfall) factors. However, the rainfall, which increased pore water pressure, reduced the mechanical strength of the slide mass, and finally drove the slope from a limited equilibrium state to a disequilibrium/unstable state, was the main triggering factor.

Concluding remarks

This study presented the physiography geological settings, deformation characteristics, as well as the triggering factors and failure mechanisms of the Sunjia landslide in Wanzhou County, China. Mainly triggered by rainfall, this landslide experienced progressive failure and produced a variety of deformation phenomenon of including a large number of tensile cracks, a surface bulge (drum hill), and ground fissures. Based on field investigations and drilling surveys, the landslide mass was divided into nine separate blocks taking into consideration their internal geological features and movements. Our study shows that the landslide exhibited a complex failure mode in which the upper part of the earth slope first deformed and slid along its geotechnical interfaces, triggering the slide of its lower part of flysch bedding rock.

Four factors, geomorphic condition, geological structure, previous slope excavations, and antecedent rainfall, had adverse effects on the failure of this complex landslide. However, we conclude that the main triggering factor was the antecedent rainfall that increased the pore water pressure and reduced the mechanical strength of the slide mass. Rainfall, coupled with the internal geological conditions such as the separated geomorphic unit, the flysch bedding slope structure of the overlying hard rock and underlying soft rock, the weak interlayers, and the previous slope excavations, drove the slope towards a disequilibrium/unstable state and final failure.

This paper presents a study of a well-observed landslide event and facilitates the understanding of the deformation characteristics and failure mechanisms of rainfall-induced complex landslides. All of this should provide new insights into landslide hazard mitigation.

Acknowledgments

We thank the Wanzhou Geological Environment Monitoring Station and the Nanjiang Hydrogeological Engineering Geological Team for providing us the valuable data. We also thank Prof. Kunlong Yin, Prof. Bo Chai from China University of Geosciences, and Prof. Steven N. Ward from University of California, Santa Cruz for their significant contributions in improving this manuscript.

Funding information

This research is supported by the National Natural Science Foundation of China (grant numbers 41907234 and 41907237), Natural Science Foundation of Shaanxi Province (CN) (grant numbers 2017JQ4010 and 2018JQ4041), Postdoctoral Research Foundation of China (CN) (grant number 2017M613033), and the Fundamental Research Funds for the Central Universities, CHD (grant numbers 300102219107 and 300102219104).

References

Baum RL, Godt JW (2010) Early warning of rainfall-induced shallow landslides and debris flows in the USA. Landslides 7(3):259–272. https://doi.org/10.1007/s10346-009-0177-0

Bonnard CH, Noverraz F (2001) Influence of climate change on large landslides: assessment of long term movements and trends. In: Proceedings of the International Conference on Landslides causes impact and countermeasures. Gluckauf, Essen, pp 121–138

Brambilla D, Ivanov VI, Longoni L, Arosio D, Papini M (2017) Geological assessment and physical model of complex landslides: integration of different techniques. In: Mikos M, Tiwari B, Yin Y, Sassa K (eds) Advancing culture of living with landslides, WLF 2017. Springer, Cham, pp 431–437

Cannon SH (1985) Rainfall conditions for abundant debris avalanches, San Francisco Bay region, California. Calif Geol 38(12):267–272

Capparelli G, Tiranti D (2010) Application of the MoniFLaIR early warning system for rainfall-induced landslides in Piedmont region (Italy). Landslides 7(4):401–410. https://doi.org/10.1007/s10346-009-0189-9

Conte E, Donato A, Troncone A (2017) A simplified method for predicting rainfall-induced mobility of active landslides. Landslides 14(1):35–45. https://doi.org/10.1007/s10346-016-0692-8

Crosta GB, Frattini P (2008) Rainfall-induced landslides and debris flows. Hydrol Process 22(4):473–477. https://doi.org/10.1002/hyp.6885

Cruden DM, Varnes DJ (1996) Landslide types and processes. In: Turner AK, Schuster RL (eds) Special report 247: landslides investigation, mitigation. National Research Council, Transportation Research Board, Washington D.C., pp 36–75

Dai FC, Lee CF (2001) Frequency-volume relation and prediction of rainfall-induced landslides. Eng Geol 59(3-4):253–266. https://doi.org/10.1016/S0013-7952(00)00077-6

Duc DM (2013) Rainfall-triggered large landslides on 15 December 2005 in Van Canh district, Binh Dinh province, Vietnam. Landslides 10:219–230. https://doi.org/10.1007/s10346-012-0362-4

Goodman RE, Kieffer DS (2000) Behavior of rock in slopes. J Geotech Geoenviron 126(8):675–684. https://doi.org/10.1061/(ASCE)1090-0241(2000)126:8(675)

Hong Y, Hiura H, Shino K, Sassa K, Suemine A, Fukuoka H, Wang G (2005) The influence of intense rainfall on the activity of large-scale crystalline schist landslides in Shikoku Island, Japan. Landslides 2(2):97–105. https://doi.org/10.1007/s10346-004-0043-z

Hungr O, Leroueil S, Picarelli L (2014) The Varnes classification of landslide types, an update. Landslides 11(2):167–194. https://doi.org/10.1007/s10346-013-0436-y

Lin F, Wu LZ, Huang RQ, Zhang H (2018) Formation and characteristics of the Xiaoba landslide in Fuquan, Guizhou, China. Landslides 15(4):669–681. https://doi.org/10.1007/s10346-017-0897-5

Luo G, Hu X, Gu C, Wang Y (2012) Numerical simulations of kinetic formation mechanism of Tangjiashan landslide. J Rock Mech Geotech Eng 4(2):149–159. https://doi.org/10.3724/SP.J.1235.2012.00149

Luo G, Hu X, Bowman ET, Liang J (2017) Stability evaluation and prediction of the dongle reactivated ancient landslide as well as emergency mitigation for the Dongla Bridge. Landslides 14:1–16. https://doi.org/10.1007/s10346-017-0796-9

Ma G, Hu X, Yin Y, Luo G, Pan Y (2018) Failure mechanisms and development of catastrophic rockslides triggered by precipitation and open-pit mining in Emei, Sichuan, China. Landslides 15(7):1401–1414. https://doi.org/10.1007/s10346-018-0981-5

Martha TR, Roy P, Govindharaj KB, Kumar KV, Diwakar PG, Dadhwal VK (2015) Landslides triggered by the June 2013 extreme rainfall event in parts of Uttarakhand state, India. Landslides 12(1):135–146. https://doi.org/10.1007/s10346-014-0540-7

Michiue M (1985) A method for predicting slope failures on cliff and mountain due to heavy rain. Nat Disaster Sci 7(1):1–12

Regmi AD, Yoshida K, Cui P, Hatano N (2017) Development of Taprang landslide, west Nepal. Landslides 14(3):929–946. https://doi.org/10.1007/s10346-016-0752-0

Reid ME (1994) A pore-pressure diffusion model for estimating landslide-inducing rainfall. J Geol 102(6):709–717. https://doi.org/10.1086/629714

Sabatakakis N, Koukis G, Mourtas D (2005) Composite landslides induced by heavy rainfalls in suburban areas: City of Patras and surrounding area, western Greece. Landslides 2(3):202–211

Santo A, Di Crescenzo G, Forte G, Papa R, Pirone M, Urciuoli G (2018) Flow-type landslides in pyroclastic soils on flysch bedrock in southern Italy: the Bosco de'Preti case study. Landslides 15(1):63–82. https://doi.org/10.1007/s10346-017-0854-3

Terzaghi K (1950) Mechanism of landslides. In: Paige S (ed) Application of geology to engineering practice. Geological Society of America, New York, pp 83–123

Varnes DJ (1958) Landslide types and processes. Highway Res Board Special Rep 29(3):20–45

Varnes DJ (1978) Slope movement types and processes. Transport Res Board Special Rep 176:11–33

Wang J (2015) Landslide risk assessment in Wanzhou County, Three Gorges Reservoir. Dissertation, China University of Geosciences (Wuhan)

Wang G, Sassa K (2003) Pore-pressure generation and movement of rainfall-induced landslides: effects of grain size and fine-particle content. Eng Geol 69(1-2):109–125. https://doi.org/10.1016/S0013-7952(02)00268-5

Xu Q, Fan X, Dong X (2012) Characteristics and formation mechanism of a catastrophic rainfall–induced rock avalanche–mud flow in Sichuan, China, 2010. Landslides 9(1):143–154. https://doi.org/10.1007/s10346-011-0278-4

Xu L, Dai FC, Chen J, Lqbal J, Qu YX (2015) Analysis of a progressive slope failure in the Xiangjiaba reservoir area, Southwest China. Landslides 11:55–66

Zhang SL, Zhu ZH, Qi SC, Hu YX, Du Q, Zhou JW (2018) Deformation process and mechanism analyses for a planar sliding in the Mayanpo massive bedding rock slope at the Xiangjiaba Hydropower Station. Landslides 15(10):2061–2073. https://doi.org/10.1007/s10346-018-1041-x

J. Wang (✉) · **L. Xiao**
School of Highway,
Chang'an University,
Xi'an, 710064, China
Email: jwang@chd.edu.cn

J. Wang · **Y. Zhu**
School of Geological Engineering and Geomatics,
Chang'an University,
Xi'an, 710064, China

J. Zhang
Tunnel and Underground Engineering Research Center of Jiangsu Province,
Nanjing, 210041, China